analytical chemistry

Article

pubs.acs.org/ac

DNA-Directed Antibody Immobilization for Enhanced Detection of Single Viral Pathogens

Elif Seymour,[†] George G. Daaboul,[‡] Xirui Zhang,[†] Steven M. Scherr,[§] Nese Lortlar Ünlü,[†,⊥] John H. Connor,[*,∥] and M. Selim Ünlü[*,†,‡]

[†]Department of Biomedical Engineering, Boston University, Boston, Massachusetts 02215, United States

[‡]Department of Electrical and Computer Engineering, Boston University, Boston, Massachusetts 02215, United States

[§]Department of Mechanical Engineering, Boston University, Boston, Massachusetts 02215, United States

[∥]Department of Microbiology, Boston University School of Medicine, Boston, Massachusetts 02218, United States

[⊥]School of Medicine, Bahcesehir University, Istanbul 34730, Turkey

Supporting Information

ABSTRACT: Here, we describe the use of DNA-conjugated antibodies for rapid and sensitive detection of whole viruses using a single-particle interferometric reflectance imaging sensor (SP-IRIS), a simple, label-free biosensor capable of imaging individual nanoparticles. First, we characterize the elevation of the antibodies conjugated to a DNA sequence on a three-dimensional (3-D) polymeric surface using a fluorescence axial localization technique, spectral self-interference fluorescence microscopy (SSFM). Our results indicate that using DNA linkers results in significant elevation of the antibodies on the 3-D polymeric surface. We subsequently show the specific detection of pseudotyped vesicular stomatitis virus (VSV) as a model virus on SP-IRIS platform. We demonstrate that DNA-conjugated antibodies improve the capture efficiency by achieving the maximal virus capture for an antibody density as low as 0.72 ng/mm^2, whereas for unmodified antibody, the optimal virus capture requires six times greater antibody density on the sensor surface. We also show that using DNA conjugated anti-EBOV GP (Ebola virus glycoprotein) improves the sensitivity of EBOV-GP carrying VSV detection compared to directly immobilized antibodies. Furthermore, utilizing a DNA surface for conversion to an antibody array offers an easier manufacturing process by replacing the antibody printing step with DNA printing. The DNA-directed immobilization technique also has the added advantages of programmable sensor surface generation based on the need and resistance to high temperatures required for microfluidic device fabrication. These capabilities improve the existing SP-IRIS technology, resulting in a more robust and versatile platform, ideal for point-of-care diagnostics applications.

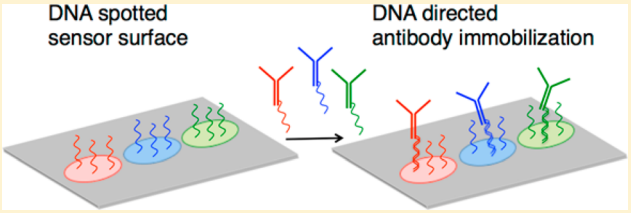

Protein microarrays are commonly used in many applications, including biomarker detection, protein−protein interaction analysis, and drug screening.[1,2] Although protein microarrays have the potential to be powerful tools for many proteomics and diagnostics applications, technical challenges related to the microarray production limit the capabilities of this technology. One challenging aspect of protein microarray production is printing the proteins onto the microarray surface. Traditional surface chemistries, such as amine-reactive surfaces, might affect antibody activity by masking the antigen binding sites due to multiple covalent interactions between the antibody and the surface.[2,3] In addition, some antibodies might lose their activity due to steric hindrance by the surface and adjacent antibody molecules.[4] Moreover, issues such as nonuniform spot morphologies and variable protein immobilization within and across microarrays affect the accuracy and robustness of the assay.[5−9] To address these issues affecting the performance of protein microarrays, researchers have explored alternative methods of protein immobilization to facilitate antibody activity and improve the assay robustness and sensitivity. Recent developments in the bioconjugation field make it possible to modify molecules easily to allow generation of versatile surface chemistries for protein immobilization. One such technique, DNA-directed immobilization (DDI), combines the robustness of DNA microarrays with the diagnostic utility of proteins through the use of protein−DNA conjugates to functionalize a DNA surface for subsequent antigen capture.[10−19]

In DDI, each antibody is encoded by a specific DNA sequence covalently attached to it. The antibodies immobilize on their complementary ssDNA probes on the sensor surface via sequence specific DNA−DNA hybridization (Figure 1b). This immobilization approach has several advantages over direct covalent attachment of antibodies. Previous studies demonstrated that DNA-tethered antibodies provide increased antigen binding capacity,[19] improved spot homogeneity,[20] and

Received: July 18, 2015
Accepted: September 17, 2015
Published: September 17, 2015

DOI: 10.1021/acs.analchem.5b02702
Anal. Chem. 2015, 87, 10505−10512

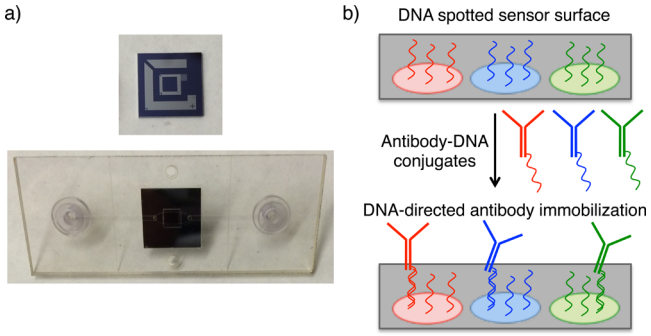

Figure 1. (a) The images of an SP-IRIS chip (10 mm × 10 mm) and an assembled microfluidic cartridge for in-liquid SP-IRIS measurements. (b) A schematic representation of SP-IRIS substrate surface with ssDNA spots and the conversion of this DNA chip into a multiplexed antibody array through hybridization of antibody−DNA conjugates.

assay reproducibility[12,20] compared to covalently attached antibodies. Using DNA linkers as a spacer between the sensor surface and the immobilized molecules potentially enhances the availability of binding sites for analyte capture by decreasing the steric hindrance and allowing more favorable orientations for binding. Moreover, DNA microarray production is less laborious than protein microarray fabrication due to easy optimization of DNA printing. Additional advantages of DNA-directed antibody immobilization include the ability to reprogram the sensor surface by using a different set of antibodies conjugated to the same DNA sequences, resilience of DNA microarrays to conditions such as the high temperature required during microfluidics fabrication, and surface regeneration by dehybridization of the antibody−DNA conjugates.

In this paper, we explore the use of DDI in combination with a simple, label-free biosensor developed by our group that can individually count and size the nanoparticles bound to capture probes on the sensor surface.[21−23] This sensor, referred to as SP-IRIS (single particle-interferometric reflectance imaging sensor), has been shown to perform sensitive and multiplexed detection of whole viruses from serum and blood samples without the need for labeling and sample preparation.[23,24] Previous studies utilizing DNA linkers for protein immobilization and subsequent antigen detection used techniques that require labeling, such as fluorescence microscopy,[12,15,20] or that consist of complicated optical platforms such as surface plasmon resonance (SPR)[11,13,17,25] and microring resonators.[19] In this work, we show the feasibility of detection of individual viruses on a DNA surface functionalized with antibody−DNA conjugates using SP-IRIS, a simple and label-free technique that has a great potential to be utilized as a rapid virus diagnostics platform.

We first evaluate the axial position of the antibodies in the antibody−DNA conjugates hybridized to surface DNA probes of different lengths on a three-dimensional (3-D) polymeric surface using spectral self-interference fluorescence microscopy (SSFM). Recently, it has been suggested that orienting and elevating the surface-immobilized antibodies improve the capture efficiency of the antibodies.[20,26,27] Therefore, it is very important to characterize the surface properties to optimize the target capture on a microarray surface. While one previous study used AFM to measure the height of a streptavidin−DNA conjugate and subsequent axial height increase upon binding of biotinylated IgG molecules,[16] this work did not address the effect of DNA probe length on the axial position of the antibody. Furthermore, this work utilized a 2-D gold substrate for DNA immobilization, which was reported to have around 50 times less immobilization than the 3-D polymeric coating used in our work.[28,29] Since increased surface coverage and 3-D structure of this polymer can greatly affect the orientation and behavior of the immobilized molecules, it is crucial to evaluate and optimize the probe properties in the context of this surface chemistry. Following optimization of the DNA probe length for the DDI technique, we compare the virus capture efficiencies of the DNA-tethered antibodies and directly spotted antibodies on the SP-IRIS platform using a vesicular stomatitis virus (VSV) pseudotype (genetically engineered VSV that expresses surface glycoprotein of Ebola virus) as a model virus. We show that the DNA-encoded antibodies improve the virus capture efficiency, resulting in an improvement of the assay sensitivity. These improvements provided by DDI will have implications for transformation of the SP-IRIS platform into a sensitive and robust technology for viral diagnostics applications.

EXPERIMENTAL SECTION

Materials and Reagents. Silicon chips (10 mm × 10 mm) with a patterned thermally grown silicon dioxide of 100 nm were purchased from Silicon Valley Microelectronics (Figure 1a). For in-liquid single particle detection experiments, the oxide was etched down to 30 nm (±2 nm) due to increased visibility of the virus particles in solution at this thickness.[30] Custom-designed, disposable microfluidic cartridges were purchased from ALine (Figure 1a). For SSFM measurements, silicon wafers with a 17.5 μm thick thermally grown oxide layer (Silicon Valley Microelectronics) were diced into 15 mm × 15 mm square chips. HPLC purified 5′-Aminated ssDNA molecules were purchased from Integrated DNA Technologies. 5′-Aminated, Atto647 fluorophore labeled 60-bp DNA was synthesized by IBA GmbH (Goettingen, Germany). Monoclonal antibodies (mAbs) against vesicular stomatitis virus (VSV) glycoprotein (8G5) and Ebola virus (EBOV) glycoprotein (13F6)[31−33] were provided by John H. Connor and Mapp Biopharmaceutical, respectively.

Preparation of Vesicular Stomatitis Virus (VSV) Pseudotypes. The VSV-based pseudotype virus expressing EBOV glycoprotein (EBOV GP) was produced by inserting the cDNA coding the relevant glycoprotein in place of VSV glycoprotein in the genome as described previously.[34] Expression of EBOV GP was confirmed by Western blotting. Virus stocks were prepared using Vero cells cultured in DMEM with 10% FCS and 1% L-glutamine. Virus titers were determined by the standard plaque assay method.

Sensor Preparation. The chips were cleaned by sonicating in acetone, rinsed with methanol and deionized (dI) water, and dried under nitrogen. The chips were then functionalized with a polymeric coating (MCP-2, Lucidant Polymers), a copoly-(DMA-NAS-MAPS) polymer described in detail elsewhere.[35] This copoly has reactive NHS groups for covalent attachment of antibodies and amine-modified DNA molecules. For the coating process, the chips were treated with oxygen plasma and then immersed in a 1× polymer solution diluted with Solution A2 (Lucidant Polymers). After 30 min, the chips were rinsed with dI water, dried with nitrogen, baked at 80 °C for 15 min, and stored in a desiccator until spotting.

Spotting of Biomolecules. Antibodies and amine-modified DNA molecules were spotted on polymer-coated

DOI: 10.1021/acs.analchem.5b02702
Anal. Chem. 2015, 87, 10505−10512

Table 1. DNA Sequences Conjugated to the Antibodies (A and B) and Their Corresponding Surface Probes (A′ and B′)[a]

antibody	oligo sequences (5′-aminated)
8G5	A: 5′ AAAAAGCCTACGAATGAACAGACTG 3′
	A′: 5′ ATATGTACCCACCGCTATTCCAGTCTGTTCATTCGTAGGC 3′
13F6	B: 5′ AAAAATACAGAGTTAGTCGCAGTGG 3′
	B′: 5′ ATCCGACCTTGACATCTCTACCACTGCGACTAACTCTGTA 3′

[a]Complementary regions between the two sequences are underlined.

chips using a Scienion S3 Flexarrayer (Berlin, Germany) piezoelectric arrayer. All antibodies were spotted in PBS with 50 mM Trehalose. All ssDNA surface probes were spotted at a concentration of 30 μM in sodium phosphate buffer (150 mM, pH = 8.5). The spotted chips were kept overnight in the spotter chamber at 67% humidity. Following the overnight immobilization, the chips were washed with 50 mM ethanolamine in 1× Tris-buffered saline (150 mM NaCl and 50 mM Tris-HCl, Fisher Scientific), pH = 8.5, for 30 min to quench the remaining NHS groups in the polymer, then washed with PBST (PBS with 0.1% Tween) for 30 min, rinsed with PBS and Nanopure water, and dried with nitrogen. DNA spots had a diameter of ∼100−120 μm, and antibody spots had a diameter of ∼150 μm.

Antibody−DNA Conjugate Synthesis. Antibody−DNA conjugates were synthesized by using Thunder-Link Oligo Conjugation Kit (Innova Biosciences). The DNA concentration used in the reaction was optimized to yield 1−2 DNA sequences per antibody. 40 μM 5′-aminated ssDNA was reacted with 1 mg/mL monoclonal antibody (8G5 or 13F6) according to the manufacturer's instructions. After conjugation, the concentration of the antibody−DNA conjugates (antibody part) was measured by the Bradford assay, and the DNA concentration was measured from the absorbance at 260 nm using NanoDrop (Thermo Scientific). Both 8G5 and 13F6 mAb conjugates were measured to have a DNA-to-antibody ratio of approximately 1.5, which indicates that some of the antibodies carried one DNA strand whereas some others carried two. DNA sequences that are used for conjugation to the mAbs (A and B sequences) and their complementary surface probes (A′ and B′) are summarized in Table 1. DNA sequences were designed by using OligoAnalyzer tool (Integrated DNA Technologies) to minimize the hairpin, self-dimer, and heterodimer structures to increase the hybridization efficiency and prevent cross hybridization. 5-bp polyA sequence was added as a spacer to the antibody-linked DNA sequences. Antibody−DNA conjugates will be denoted in the text by adding the letter representing the DNA sequence to the antibody name as follows: 8G5 − DNA "A" and 13F6 − DNA "B", for antibodies against wild-type VSV (WT-VSV) and EBOV GP pseudotyped VSV, respectively.

Optical Setup and Data Analysis. Surface density of immobilized antibodies was measured using the interferometric reflectance imaging sensor (IRIS), an interferometric biosensor that can quantify biomass accumulation on Si/SiO_2 substrates in a high-throughput microarray format.[29,36,37] In this setup, four different wavelength LEDs illuminate the substrate sequentially and the reflected light intensities are recorded by a CCD. The intensity values at each wavelength for each pixel are then fitted to a reflectivity curve from which the optical thickness of the transparent film (SiO_2 plus any biomolecule layer) is obtained.[38] The thickness values for each pixel are then mapped to a grayscale image. This image is analyzed by custom software where the thickness of each spot is calculated by subtracting the average thickness of a circular area around the spot (background) from the average thickness of a circular region drawn in the spot covering 80% of the spot. The spot thicknesses are converted to biomass densities using the conversion factor of 1 nm = 1.2 ng/mm^2 for IgG molecules and 0.8 ng/mm^2 for DNA molecules.[29]

SSFM measurements were performed to determine the optimal DNA probe length for the DDI method. SSFM can determine the average axial height of fluorophores above a Si/SiO_2 layered substrate from the spectral oscillations caused by the interference between direct and reflected waves of emitted fluorescence.[39] SSFM has been shown to determine the average axial position of DNA molecules tagged with fluorophores with subnanometer resolution.[39,40] The optical setup, data acquisition, and the fluorescence spectra processing of SSFM to obtain average axial fluorophore heights have been previously described in detail elsewhere.[39,41]

All virus detection experiments were performed in-solution using SP-IRIS and 30 nm-oxide chips mounted into a microfluidic cartridge (Figure 1a) via a pressure sensitive adhesive (PSA). Assembled cartridges were placed on the SP-IRIS stage and connected to a syringe pump (Harvard Apparatus, PHD 2000). A flow rate of 3 μL/min was used for all in-liquid experiments. SP-IRIS uses a single wavelength to illuminate the substrate and a high-magnification objective (40×, 0.9 NA) to image the individual particles directly on the camera. Captured particles appear as bright dots in the image. Background normalized intensities of these dots are correlated to particle size via a forward-model.[21] The focus was maintained using CRISP autofocus system (Applied Scientific Instrumentation, MFC-2000) during scanning of an array of spots. SP-IRIS images were analyzed using custom software that identifies the particles based on local intensity peaks and their correlation with the Gaussian-type intensity profile. To determine the captured virus density in a spot, we find the particles in the appropriate size range expected for the virus of interest in the pre- and postincubation images. We then subtract the preincubation particle counts from the post-incubation particle counts and divide by the spot area. The signal is expressed as a density to be able to compare the signals between spots of different size.

Determination of Axial Position of Antibody−DNA Conjugates Hybridized to Surface-Immobilized DNA of Different Lengths. 20mer, 40mer, and 60mer ssDNA surface probes and 8G5 antibody were spotted on a polymer coated SSFM chip along with a control DNA sequence with a fluorophore tag (Atto647) on the surface-proximal end. The spotted and washed chip was incubated with 5 μg/mL 8G5 − DNA "A" conjugate for 1 h on a shaker, washed with PBS twice, washed with 0.5 M sodium nitrate buffer twice, and then dipped in cold 0.1 M sodium nitrate buffer.[42] The chip was then incubated with 10 μg/mL fluorescent secondary antibody (Alexa Fluor @635 goat antimouse IgG, Life Technologies) for 1 h and washed as before. The chip was assembled into a

DOI: 10.1021/acs.analchem.5b02702
Anal. Chem. 2015, 87, 10505−10512

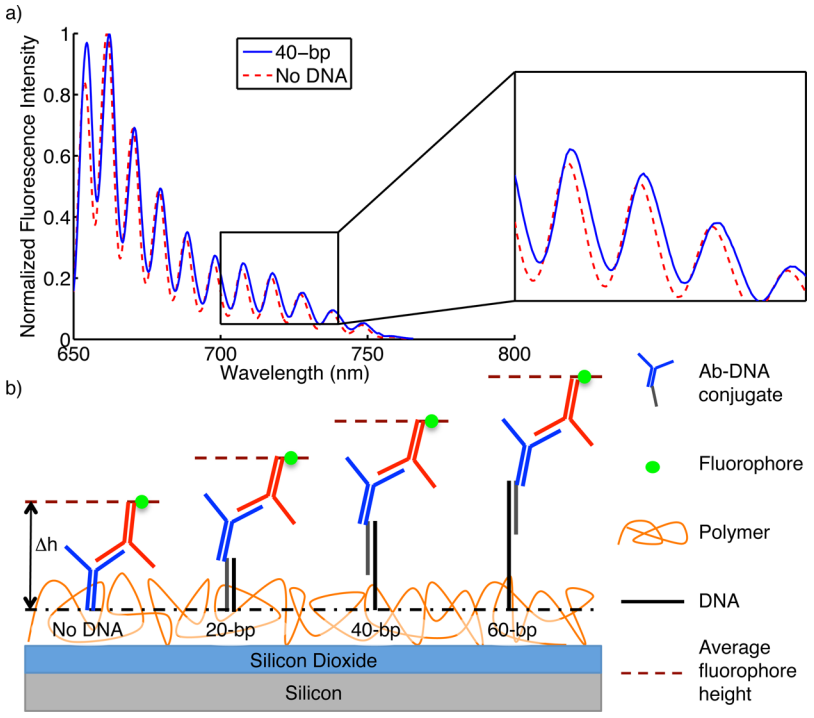

Figure 2. (a) The fluorescence emission spectra of the fluorophores measured from a single spot for both the direct immobilization (dashed line) and 40-bp DNA cases (solid line). Other probe lengths were omitted for simplicity. (b) A schematic representation of the SSFM substrate showing the antibodies immobilized on DNA probes of different lengths. Baseline film thickness (shown by the dash-dotted line) is measured by immobilizing a control DNA sequence with a surface-proximal fluorophore. Δh represents the average axial height of the fluorophores from the baseline film thickness.

customized flow cell[41] which was fixed onto a two-axis positioning microstage. The flow cell was filled with PBS, and the fluorescence emission was recorded using SSFM for 18 replicate spots for each probe type.

Surface Antibody Density Measurements and Subsequent in-Liquid Virus Detection Experiments. For investigating the effect of antibody density on the captured virus density, 13F6 mAb was spotted at six different concentrations (0.3, 0.9, 2.0, 3.1, 4.3, and 5.3 mg/mL) with 6 replicate spots for each concentration on both a 100 nm-oxide chip for biomass quantification and a 30 nm-oxide chip for in-liquid virus detection. To create a varying degree of immobilization for 13F6 − DNA "B" conjugate, B′ probe was spotted at 6 different concentrations (3, 6, 12, 18, 24, 30 μM) on 30 nm- and 100 nm-oxide chips. Two separate SP-IRIS chips (one 30 nm-oxide and one 100 nm-oxide) were also spotted with a noncomplementary DNA sequence and 8G5 mAb as negative control chips.

After spotting, the chips were washed as mentioned before and 100 nm-oxide chips were imaged with IRIS to obtain the thicknesses of ssDNA and directly immobilized antibody spots. Next, both the DNA and the negative control chips were incubated with 13F6 − DNA "B" conjugate (at 5 μg/mL in PBS with 1% BSA) for 1 h in a 24-well plate on a shaker. After the incubation ended, the chips were washed with PBS twice and with 0.5 M sodium nitrate buffer twice, then dipped in cold 0.1 M sodium nitrate buffer, and dried with nitrogen. The increase in spot thickness due to the hybridization of 13F6 − DNA "B" conjugate was measured by imaging the chip again with IRIS and subtracting the initial ssDNA spot thickness from the posthybridization spot thickness for each spot. We further subtracted the thickness contributed by the DNA sequences attached to the antibody to determine the antibody thickness on a given DNA spot.

Single virus detection experiments were done in-liquid by mounting the antibody and DNA chips into microfluidic cartridges. For the DNA spotted chip, 13F6 − DNA "B" conjugate was flowed at a concentration of 5 μg/mL in PBS with 1% BSA for 1 h followed by a 400 μL PBS wash step. Then, SP-IRIS images of 6 spots for each probe density were acquired to obtain the preincubation particle counts. Next, 10^4 PFU/mL EBOV GP pseudotyped VSV was flowed over the chip for 30 min; the channel was washed with 400 μL of PBS, and the spots were imaged with SP-IRIS again. For the antibody chip, the preincubation images were acquired after filling the channel with PBS with 1% BSA. The chip was then incubated with the same virus dilution for 30 min, and image acquisition was performed as described for the DNA chip. The images were then analyzed for bound virus particles for each spot. The 30 nm-oxide negative control chip was mounted in a different cartridge and incubated first with the 13F6 − DNA "B" conjugate and then the same virus dilution as the two previous chips.

Determination of Limit of Detection (LOD) for EBOV-Pseudotyped VSV Detection. For the comparison of directly immobilized and DNA-conjugated 13F6 antibody in terms of LOD for EBOV GP pseudotyped VSV detection, 13F6 mAb and 5′-amine-modified B′ sequence were spotted on 30 nm-oxide SP-IRIS chips at a concentration of 3 mg/mL and 30 μM, respectively. Spotted and washed chips were mounted in the microfluidic cartridges, and 5 μg/mL of 13F6 − DNA "B" conjugate (in PBS with 1% BSA) was flowed for 30 min. After washing the channel with 400 μL of PBS, the EBOV-pseudotyped VSV in PBS with 1% BSA was flowed for 1 h.

DOI: 10.1021/acs.analchem.5b02702
Anal. Chem. 2015, 87, 10505−10512

Five different titers in the range of 500−32000 PFU/mL were tested. The SP-IRIS image acquisitions were done before the virus flow (in PBS with 1% BSA) and at the 15th and 60th minutes of the incubation by scanning 5 replicate spots for both directly spotted 13F6 spots and DNA spots.

RESULTS AND DISCUSSION

Optimization of Antibody Height from the Sensor Surface. We first investigated the axial positions of antibodies immobilized on a 3-D polymeric surface via both direct covalent attachment and DDI. Our purpose was both to compare the axial positions of directly immobilized and DNA-tethered antibodies and to optimize the DNA probe length for the virus detection experiments. To this end, a polymer coated SSFM chip was spotted with 8G5 antibody, ssDNA probes of three different lengths (20-bp, 40-bp, and 60-bp) and a control ssDNA sequence, 18 replicate spots for each condition. The chip was first incubated with 8G5 − DNA "A" conjugate, which is fully complementary to the 20-bp probe (except for the 5-bp spacer sequence) and partially complementary to 40-bp and 60-bp probes, and then with fluorophore labeled secondary antibody (Figure 2b). Figure 2a shows the spectral interference signature of the ensemble of fluorophores from a single spot for two different cases: directly immobilized and DNA tethered (40-bp) 8G5 antibody. Figure 3 demonstrates the effect of

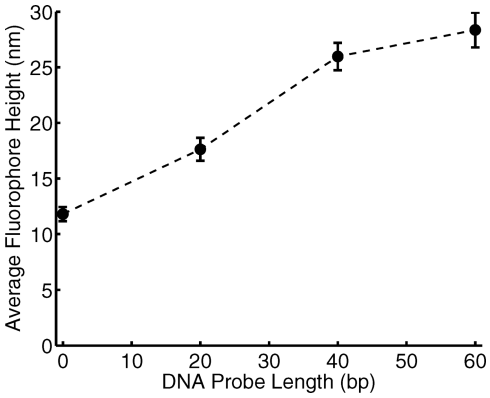

Figure 3. Effect of the DNA probe length on the axial position of the antibody. Average fluorophore heights (Δh) were measured in PBS using SSFM and plotted as a function of DNA probe length. 0-bp corresponds to directly immobilized antibody. Data points are connected using a dashed line to emphasize the significant height increase between the 20-bp and 40-bp DNA probes. Error bars indicate the variation among 18 replicate spots.

DNA probe length on the average fluorophore heights that are calculated by subtracting the average polymer thickness from the fluorophore-to-surface distance to yield the average axial positions of 2° antibody−1° antibody−DNA complexes. Average polymer thickness (average height of binding sites in the polymeric scaffold) was measured from the control DNA sequence labeled with Atto647 fluorophore at the surface-proximal end. Without any DNA linkers, antibody complex had an average axial height of 11.8 nm, which is in good agreement with our previous SSFM results that showed an average ∼6 nm axial height for Cy3-labeled 8G5 mAb directly spotted on the polymer (data not shown). 20mer DNA tether increased the average height of 2° antibody−1° antibody complex by 5.8 nm, which is smaller than the expected increase for a fully extended length of a 20-bp DNA (6.8 nm). This is due to the thermal fluctuations causing different orientations and random rotations for short DNA molecules in the polymeric scaffold.[41] Moreover, DNA molecules penetrate into the polymer and distribute themselves axially depending on the length of the DNA. Shorter DNA sequences penetrate into the polymeric scaffold deeper, which might also have contributed to reduced average fluorophore height. 40mer DNA probe, 20-bp of which is complementary to the Ab−DNA conjugate, elevated the antibody a further 8.3 nm, which is more than what is expected from the addition of another 20-bp long DNA. This large increase in height for the 40-bp spacer is due to the fact that longer DNA strands immobilize at higher axial positions in the polymer scaffold and steric hindrance and electrostatic repulsion orient the DNA molecules. The fluorophore height increased an additional ∼2.4 nm for the 60-bp probe case. This small height increase is most likely due to the fact that the ssDNA portion of the 60-bp (40-bp long) assumes a random coil conformation, decreasing the height of the antibody.[43] We selected the 40-bp as the optimal probe height since it provided substantially greater elevation of the antibody from the surface compared to the 20mer probe. 60-bp probe does not provide a significant advantage over 40-bp probe, and also, it is easier to overcome design challenges such as formation of secondary structures with the selection of a shorter DNA probe.

Comparing Virus Capture Efficiencies of Directly Immobilized and DNA-Tethered Antibodies. For this experiment, both types of IRIS measurements (biomass quantification and single-particle imaging) were performed and the correlation between the surface antibody density and the captured virus density was investigated for an Ebola virus glycoprotein monoclonal antibody (13F6) that was either directly immobilized on the sensor chip or tethered to surface via DNA linkers. The EBOV-pseudotyped VSV titer used for this experiment was 10^4 PFU/mL. This titer was selected since it provides a good amount of signal without saturating the spot images with particles, allowing the particle detection algorithm to find the individual particles more accurately. A plaque forming unit does not reflect the actual number of viral particles in a virus sample. The particle to PFU ratio for viruses varies widely. For EBOV GP pseudotyped VSV, we estimate a conversion factor of at least 100; i.e., 1 PFU corresponds to about 100 virus particles.

In Figure 4b, the average spot thicknesses (1 nm of spot thickness corresponds to 1.2 ng/mm^2 of surface antibody density) obtained from biomass measurements were plotted against the average captured virus densities for different degrees of immobilization (n = 6 replicate spots). For the directly immobilized antibody, the captured virus density increases linearly with the immobilized antibody density. For the DNA-tethered antibody (13F6 − DNA "B"), on the other hand, captured virus density reaches the maximum level with an antibody spot height as low as 0.6 nm (corresponding to a surface density of 0.72 ng/mm^2). Directly immobilized antibody requires approximately 6 times denser immobilization to reach the maximum virus capture. Further, the maximum virus density for the DNA-conjugated antibody is higher than that of the unmodified antibody. The fact that the unmodified antibodies cannot reach the virus capture level of DNA-linked antibodies even at the highest surface density provides evidence for the hypothesis that not all of the antibodies on the surface remain functional, perhaps due to the blockage of binding sites or the steric hindrance between the antibody molecules. DNA-conjugated antibodies, on the other hand, are tethered to the

DOI: 10.1021/acs.analchem.5b02702
Anal. Chem. 2015, 87, 10505−10512

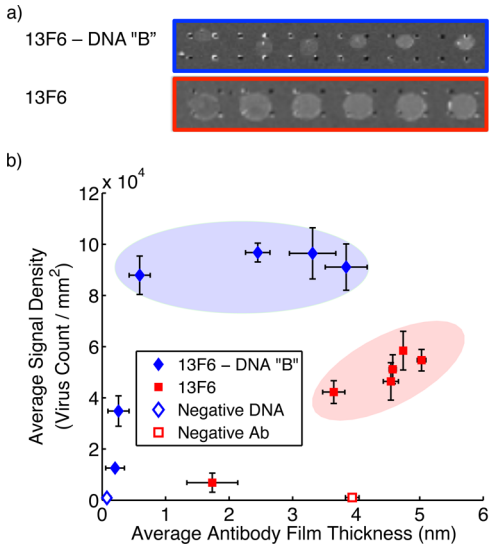

Figure 4. (a) Two representative rows from the fitted IRIS images showing the varying probe densities for 13F6 − DNA "B" conjugate (top) and unmodified 13F6 antibody (bottom). Gray scale images represent the biofilm thicknesses on the chip: The spots with a higher antibody surface density are brighter. A negative control antibody and a noncomplementary DNA sequence were also spotted on a separate chip (not shown). (b) Effect of surface antibody density (1 nm = 1.2 ng/mm^2) on virus capture for both unmodified and DNA-conjugated antibody. Average virus densities obtained from SP-IRIS images were plotted against the average antibody film thickness obtained from IRIS biomass measurements (n = 6 spots). The ellipses indicate the range of surface antibody densities where the optimal virus capture occurs.

surface via one or two DNA linkers, which can help expose the antigen binding sites. Also, the significant elevation of the antibodies from the surface, as shown by our SSFM experiments (∼14 nm), may provide increased flexibility and decreased steric hindrance from the surface and adjacent antibody molecules. Overall, these results indicate that the DNA-conjugated antibodies show increased capture efficiency compared to covalently attached antibodies. Moreover, the fact that the optimal performance is observed over a large range of immobilization densities has implications for the increased reproducibility and robustness of the assay.

Specificity of the antibody−DNA conjugates was also evaluated by first functionalizing the DNA surface with 8G5 − DNA "A" and 13F6 − DNA "B" conjugates and flowing the WT-VSV and EBOV-pseudotyped VSV sequentially in the microfluidic channel. Our results demonstrate the sequence-specific immobilization of the two antibody−DNA conjugates and subsequent specific detection of two types of viruses (Figures S1 and S2).

Determining the Assay Sensitivity for EBOV-Pseudotyped VSV Detection: Comparing Directly Immobilized and DNA-Conjugated Antibodies. To determine how the improvement in the capture efficiency of DNA-conjugated 13F6 antibody affects the assay sensitivity, we spotted B′ sequence and 13F6 antibody on SP-IRIS chips. We performed EBOV-GP pseudotyped VSV detection experiments using different virus titers and incubation times with both the covalent and the DNA-directed immobilization approaches. We inspected the covalently attached antibody spots to ensure that the immobilization is in the optimal range (4−5 nm). We tested different virus titers in the clinically relevant range (10^3−10^4 PFU/mL) and different incubation times (15, 30, and 60 min). For all experiments, we first performed DNA-directed immobilization of 13F6 antibody by flowing the 13F6 − DNA "B" (at 5 μg/mL in PBS with 1% BSA) for 30 min. Next, we washed the channel with 400 μL of PBS, flowed EBOV pseudotyped VSV, and analyzed the virus densities on the DNA-tethered and covalently attached 13F6 spots.

Figure 5 shows the comparison of captured virus densities for the two types of immobilization techniques. Each data point, indicated by a letter next to it, represents captured virus densities obtained from an independent experiment. (The experimental conditions for each experiment are shown in the table.) These results show that the capture efficiency of the DNA-linked antibodies is higher than that of the covalently attached antibodies across different experiments performed with various virus titers and incubation times. Capture efficiency improvements are reflected in the #-fold increase values (Figure 5). The increase in the capture efficiency is much higher at low titers of the virus and at shorter incubation times, shown by A, B, C, and D data points. This is an expected result since, at lower virus concentrations, there are fewer targets available for binding and the number of binding events

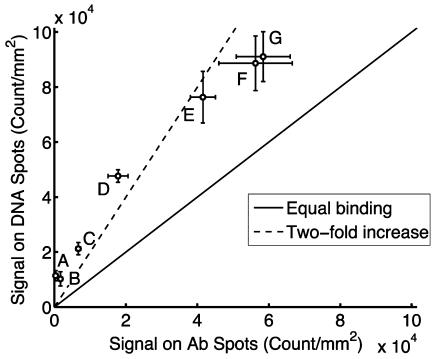

Experiment	Virus titer (PFU/ml)	Incubation time (min)	#-fold increase
A	1x10^3	60	34.3
B	2x10^3	15	6.1
C	8x10^3	15	3.2
D	1x10^4	15	2.7
E	1x10^4	30	1.8
F	1x10^4	30	1.6
G	1x10^4	30	1.6

Figure 5. Comparing captured virus densities of covalently immobilized and DNA-tethered antibodies. Each data point corresponds to a different experiment using a certain virus concentration and incubation time. Error bars show the variation between 6 spots for a given experiment. Experimental conditions for each experiment are shown in the table. #-fold increase values (the average virus density on the DNA spots divided by the average density on the direct antibody spots) for each experiment are also given. The solid line represents equal binding capacity whereas the dashed line represents a 2-fold increase in binding by DNA-tethered antibody. DNA-conjugated 13F6 demonstrates higher capture efficiency for all of the experiments. For low virus concentrations and shorter incubation times, the virus capture ratio gets larger, indicating the increased assay sensitivity.

DOI: 10.1021/acs.analchem.5b02702
Anal. Chem. 2015, 87, 10505−10512

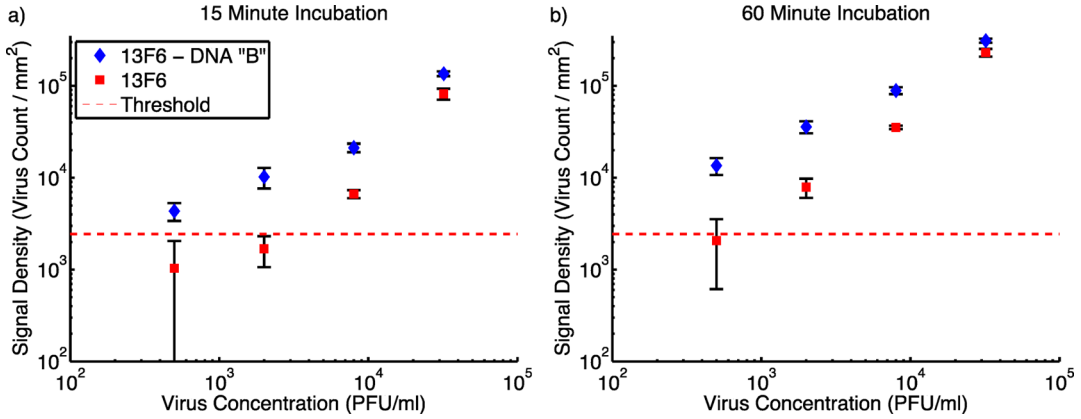

Figure 6. Comparison of directly immobilized antibodies with DNA-conjugated counterparts in a EBOV-GP pseudotyped VSV detection experiment with serially diluted virus samples. Captured virus densities obtained from SP-IRIS measurements were plotted against the virus titer for a (a) 15 min incubation and (b) 60 min incubation. Virus solutions were prepared by 4-fold serial dilutions from 3.2×10^4 PFU/mL sample. Detection threshold, shown as the dashed line, was calculated as the mean virus density of the five 13F6 spots plus three standard deviations from a chip incubated with the blank solution (PBS with 1% BSA).

decreases significantly, decreasing the capture efficiency. Therefore, it becomes more critical for the immobilized antibodies to be available for binding. As discussed earlier, DNA-conjugated antibodies are elevated significantly from the surface into the solution, increasing their accessibility. Moreover, they are more likely to expose their binding sites due to increased flexibility attributed by the DNA linkers. Similarly, the flexibility and accessibility plays an important role in the faster binding of the DNA-conjugated antibodies, resulting in improved binding capacity at shorter incubation times for a given concentration (D vs E). As the virus concentration and incubation time increase, the number of binding events increases and the differences between the capture efficiencies become smaller (E, F, and G); however, DDI still provides significant improvement in the virus capture efficiency.

We also performed EBOV-GP pseudotyped VSV detection with serially diluted virus samples in the range of 32 000−500 PFU/mL to determine the limit of detection (LOD) using both immobilization techniques. Figure 6 shows the detected virus density for directly immobilized and DNA-conjugated 13F6 spots as a function of virus concentration for 15 min and 1 h incubations (n = 5 spots). DNA-conjugated 13F6 captures significantly more viruses compared to directly immobilized 13F6 for all titers of the virus for both time points. This is consistent with our previous results (Figure 5). Detection thresholds were calculated as the average of the signal densities from five 13F6 spots (both direct and DNA-conjugated 13F6 spots) incubated with blank sample plus three times the standard deviation. Since the threshold values were similar, the larger of the two values was used.

For the lowest titer tested (500 PFU/mL), the DNA-conjugated antibody spots showed significant detection (an average signal density of 4350 particles/mm^2) in 15 min (Figure 6a), which is above the threshold density of 3098 particles/mm^2. Directly immobilized 13F6, on the other hand, did not show a signal above the threshold for either the 500 PFU/mL or the 2000 PFU/mL dilutions in 15 min. For the 60 min incubation, 2000 PFU/mL titer became detectable by the direct antibody immobilization whereas the signal for 500 PFU/mL still remained in the noise level (Figure 6b). For virus diagnostics, it is important that the signal detected is well above the threshold to avoid type II error (a false negative). Therefore, our results suggest that increased virus capture obtained with the use of DNA linkers improves the assay sensitivity and accuracy for short assay times. Our results show that the DNA-conjugated 13F6 has an LOD of 500 PFU/mL in 15 min whereas LOD for the direct antibody is 8000 PFU/mL in 15 min. For a 60 min incubation, LOD can be predicted as 2000 PFU/mL for directly immobilized 13F6. These results indicate that the DDI technique improves the sensitivity of EBOV-GP pseudotyped VSV detection by an order of magnitude for a 15 min incubation.

CONCLUSION

We demonstrated feasibility of DNA-directed antibody immobilization for detection of individual viruses on a microarray surface using the SP-IRIS platform. We first characterized the elevation of the antibody−DNA conjugates from the surface on a 3-D polymeric scaffold and determined the optimal length of the DNA linkers. Next, we demonstrated that DDI improves the capture efficiency of the antibodies for EBOV-GP pseudotyped VSV detection. Increased capture efficiency has been shown to improve the assay sensitivity by an order of magnitude for a short incubation time (15 min). Therefore, application of the DDI technique to SP-IRIS can accelerate the development of a rapid and sensitive point-of-care diagnostics platform. The DDI technique also offers high manufacturing capacity and quality since DNA microarrays are easier to prepare than protein microarrays and are highly reproducible. A large quantity of DNA chips can be produced and stored at room temperature for an extended period of time without denaturation. When there is need for viral diagnostics, especially in urgent outbreak situations, these DNA microarrays can be functionalized quickly according to the need. The DDI technique can also help immobilize the capture probes that show poor immobilization or poor spot morphologies, thereby improving the assay sensitivity and accuracy.

ASSOCIATED CONTENT

Supporting Information

The Supporting Information is available free of charge on the ACS Publications website at DOI: 10.1021/acs.analchem.5b02702.

DOI: 10.1021/acs.analchem.5b02702
Anal. Chem. 2015, 87, 10505−10512

Validation of specificity of antibody−DNA conjugates on SP-IRIS; Fig S1: Specificity of two antibody−DNA conjugate; Fig S2: SP-IRIS images of DNA spots from sequential incubation with two types of viruses (PDF)

AUTHOR INFORMATION

Corresponding Authors

*E-mail: selim@bu.edu.

*E-mail: jhconnor@bu.edu.

Notes

The authors declare no competing financial interest.

ACKNOWLEDGMENTS

We would like to thank Larry Zeitlin (Mapp Biopharmaceutical) for kindly sharing antibody reagents used in this work. We also thank Erik Paul Carter for his assistance with virus stock preparation and plaque assays. This work was supported by R01AI1096159 to J.H.C. and M.S.U.

REFERENCES

(1) MacBeath, G.; Schreiber, S. L. *Science* **2000**, *289*, 1760−1763.

(2) Sun, H.; Chen, G. Y. J.; Yao, S. Q. *Chem. Biol.* **2013**, *20*, 685−699.

(3) Schwenk, J. M.; Lindberg, J.; Sundberg, M.; Uhlén, M.; Nilsson, P. *Mol. Cell. Proteomics* **2007**, *6*, 125−132.

(4) Peluso, P.; Wilson, D. S.; Do, D.; Tran, H.; Venkatasubbaiah, M.; Quincy, D.; Heidecker, B.; Poindexter, K.; Tolani, N.; Phelan, M.; Witte, K.; Jung, L. S.; Wagner, P.; Nock, S. *Anal. Biochem.* **2003**, *312*, 113−124.

(5) Nielsen, U. B.; Geierstanger, B. H. *J. Immunol. Methods* **2004**, *290*, 107−120.

(6) Seurynck-Servoss, S. L.; White, A. M.; Baird, C. L.; Rodland, K. D.; Zangar, R. C. *Anal. Biochem.* **2007**, *371*, 105−115.

(7) Deng, Y.; Zhu, X. Y.; Kienlen, T.; Guo, A. *J. Am. Chem. Soc.* **2006**, *128*, 2768−2769.

(8) Mace, C. R.; Yadav, A. R.; Miller, B. L. *Langmuir* **2008**, *24*, 12754−12757.

(9) Romanov, V.; Davidoff, S. N.; Miles, A. R.; Grainger, D. W.; Gale, B. K.; Brooks, B. D. *Analyst* **2014**, *139*, 1303−1326.

(10) Niemeyer, C. M.; Boldt, L.; Ceyhan, B.; Blohm, D. *Anal. Biochem.* **1999**, *268*, 54−63.

(11) Ladd, J.; Boozer, C.; Yu, Q.; Chen, S.; Homola, J.; Jiang, S. *Langmuir* **2004**, *20*, 8090−8095.

(12) Wacker, R.; Niemeyer, C. M. *ChemBioChem* **2004**, *5*, 453−459.

(13) Boozer, C.; Ladd, J.; Chen, S.; Jiang, S. *Anal. Chem.* **2006**, *78*, 1515−1519.

(14) Bailey, R. C.; Kwong, G. A.; Radu, C. G.; Witte, O. N.; Heath, J. R. *J. Am. Chem. Soc.* **2007**, *129*, 1959−1967.

(15) Fan, R.; Vermesh, O.; Srivastava, A.; Yen, B. K. H.; Qin, L.; Ahmad, H.; Kwong, G. A.; Liu, C.-C.; Gould, J.; Hood, L.; Heath, J. R. *Nat. Biotechnol.* **2008**, *26*, 1373−1378.

(16) Bano, F.; Fruk, L.; Sanavio, B.; Glettenberg, M.; Casalis, L.; Niemeyer, C. M.; Scoles, G. *Nano Lett.* **2009**, *9*, 2614−2618.

(17) Fruk, L.; Kuhlmann, J.; Niemeyer, C. M. *Chem. Commun. (Cambridge, U. K.)* **2009**, 230−232.

(18) Schroeder, H.; Adler, M.; Gerigk, K.; Müller-Chorus, B.; Götz, F.; Niemeyer, C. M. *Anal. Chem.* **2009**, *81*, 1275−1279.

(19) Washburn, A. L.; Gomez, J.; Bailey, R. C. *Anal. Chem.* **2011**, *83*, 3572−3580.

(20) Wacker, R.; Schröder, H.; Niemeyer, C. M. *Anal. Biochem.* **2004**, *330*, 281−287.

(21) Daaboul, G. G.; Yurt, A.; Zhang, X.; Hwang, G. M.; Goldberg, B. B.; Ünlü, M. S. *Nano Lett.* **2010**, *10*, 4727−4731.

(22) Yurt, A.; Daaboul, G. G.; Connor, J. H.; Goldberg, B. B.; Ünlü, M. S. *Nanoscale* **2012**, *4*, 715−726.

(23) Daaboul, G. G.; Lopez, C. A.; Yurt, A.; Goldberg, B. B.; Connor, J. H.; Ünlü, M. S. *IEEE J. Sel. Top. Quantum Electron.* **2012**, *18*, 1422−1433.

(24) Daaboul, G. G.; Lopez, C. A.; Chinnala, J.; Goldberg, B. B.; Connor, J. H.; Ünlü, M. S. *ACS Nano* **2014**, *8*, 6047−6055.

(25) Boozer, C.; Ladd, J.; Chen, S.; Yu, Q.; Homola, J.; Jiang, S. *Anal. Chem.* **2004**, *76*, 6967−6972.

(26) Cha, T.; Guo, A.; Zhu, X. Y. *Proteomics* **2005**, *5*, 416−419.

(27) Guilleaume, B.; Buneß, A.; Schmidt, C.; Klimek, F.; Moldenhauer, G.; Huber, W.; Arlt, D.; Korf, U.; Wiemann, S.; Poustka, A. *Proteomics* **2005**, *5*, 4705−4712.

(28) Steel, a B.; Levicky, R. L.; Herne, T. M.; Tarlov, M. J. *Biophys. J.* **2000**, *79*, 975−981.

(29) Ozkumur, E.; Yalçin, A.; Cretich, M.; Lopez, C. a; Bergstein, D. a; Goldberg, B. B.; Chiari, M.; Unlü, M. S. *Biosens. Bioelectron.* **2009**, *25*, 167−172.

(30) Scherr, S. M.; Daaboul, G. G.; Trueb, J. T.; Sevenler, D.; Fawcett, H. E.; Fawcett, B. B.; Connor, J. H.; Unlu, M. S. 2015, submitted for publication.

(31) Wilson, J. A.; Hevey, M.; Bakken, R.; Guest, S.; Bray, M.; Schmaljohn, A. L.; Hart, M. K. *Science* **2000**, *287*, 1664−1666.

(32) Zeitlin, L.; Pettitt, J.; Scully, C.; Bohorova, N.; Kim, D.; Pauly, M.; Hiatt, a.; Ngo, L.; Steinkellner, H.; Whaley, K. J.; Olinger, G. G. *Proc. Natl. Acad. Sci. U. S. A.* **2011**, *108*, 20690−20694.

(33) Olinger, G. G.; Pettitt, J.; Kim, D.; Working, C.; Bohorov, O.; Bratcher, B.; Hiatt, E.; Hume, S. D.; Johnson, a. K.; Morton, J.; Pauly, M.; Whaley, K. J.; Lear, C. M.; Biggins, J. E.; Scully, C.; Hensley, L.; Zeitlin, L. *Proc. Natl. Acad. Sci. U. S. A.* **2012**, *109*, 18030−18035.

(34) Mire, C. E.; Geisbert, J. B.; Versteeg, K. M.; Mamaeva, N.; Agans, K. N.; Geisbert, T. W.; Connor, J. H. *J. Infect. Dis.* **2015**, *212*, S384−S388.

(35) Cretich, M.; Pirri, G.; Damin, F.; Solinas, I.; Chiari, M. *Anal. Biochem.* **2004**, *332*, 67−74.

(36) Daaboul, G. G.; Vedula, R. S.; Ahn, S.; Lopez, C. A.; Reddington, A.; Ozkumur, E.; Ünlü, M. S. *Biosens. Bioelectron.* **2011**, *26*, 2221−2227.

(37) Lopez, C. A.; Daaboul, G. G.; Vedula, R. S.; Özkumur, E.; Bergstein, D. A.; Geisbert, T. W.; Fawcett, H. E.; Goldberg, B. B.; Connor, J. H.; Ünlü, M. S. *Biosens. Bioelectron.* **2011**, *26*, 3432−3437.

(38) Ozkumur, E.; Needham, J. W.; Bergstein, D. a; Gonzalez, R.; Cabodi, M.; Gershoni, J. M.; Goldberg, B. B.; Unlü, M. S. *Proc. Natl. Acad. Sci. U. S. A.* **2008**, *105*, 7988−7992.

(39) Moiseev, L.; Cantor, C. R.; Aksun, M. I.; Dogan, M.; Goldberg, B. B.; Swan, a. K.; Ünlü, M. S. *J. Appl. Phys.* **2004**, *96*, 5311.

(40) Moiseev, L.; Unlü, M. S.; Swan, A. K.; Goldberg, B. B.; Cantor, C. R. *Proc. Natl. Acad. Sci. U. S. A.* **2006**, *103*, 2623−2628.

(41) Zhang, X.; Daaboul, G. G.; Spuhler, P. S.; Freedman, D. S.; Yurt, A.; Ahn, S.; Avci, O.; Ünlü, M. S. *Analyst* **2014**, *139*, 6440−6449.

(42) Hill, H. D.; Mirkin, C. a. *Nat. Protoc.* **2006**, *1*, 324−336.

(43) Singh-Zocchi, M.; Dixit, S.; Ivanov, V.; Zocchi, G. *Proc. Natl. Acad. Sci. U. S. A.* **2003**, *100*, 7605−7610.

DOI: 10.1021/acs.analchem.5b02702
Anal. Chem. 2015, 87, 10505−10512